Analysis of heavy-ion fusion reactions at extreme sub-barrier energies

C. L. Jiang, H. Esbensen, B. B. Back, R. V. F. Janssens, and K. E. Rehm
Physics Division, Argonne National Laboratory, Argonne, Illinois 60439, USA
(Received 21 October 2003; published 20 January 2004)

A coupled-channels analysis has been carried out for fusion reactions in the system ^{60}Ni+^{89}Y. It demonstrates that conventional coupled-channels calculations are unable to reproduce the unexpected steep falloff of the recently measured cross sections at extreme sub-barrier energies. Heavy-ion fusion excitation functions are also analyzed in terms of the *S* factor, as this offers a pragmatic way to study fusion behavior in the energy regime of interest. It is shown that the steep falloff in cross section observed in several heavy-ion systems translates into a maximum of the *S* factor. The energies where the maximum occurs can be parametrized with a simple empirical formula. The parametrization, which is derived here for rather stiff heavy-ion systems, provides an upper limit for reactions involving softer nuclei.

DOI: 10.1103/PhysRevC.69.014604 PACS number(s): 24.10.Eq, 25.70.Jj

I. INTRODUCTION

The asymptotic behavior of reaction cross sections at very low energy is a critical issue for calculating reaction rates of astrophysical interest. Recently, it was pointed out that fusion cross sections for several heavy-ion systems show an unexpected behavior at very low energies [1], with a much steeper falloff than obtained in conventional coupled-channels calculations [2], or from Wong's formula [3]. In the present work, we first take a detailed look at the fusion of ^{60}Ni+^{89}Y, the system originally reported in Ref. [1], but not analyzed in terms of coupled-channels calculations. We then relate the study of fusion reactions at extreme sub-barrier energies to a representation in terms of the *S* factor. This factor, which in the past has been successfully applied to fusion reactions with lighter ions at low energies, proves to be an alternative, pragmatic way of characterizing and exploring the behavior of heavy-ion fusion cross sections in the energy domain of interest. To our surprise, a maximum appears systematically in the evolution of *S* with the energy *E* for all systems exhibiting the steep falloff described above. This maximum occurs at values of *E* corresponding to a rather high excitation energy in the compound nucleus.

II. COUPLED-CHANNELS CALCULATIONS

The experimental cross sections for ^{60}Ni+^{89}Y [1] are compared in Fig. 1(a) with three calculations. The solid and dotted curves are the results of coupled-channels calculations which are performed in the rotating target frame approximation [4] and include the low-lying quadrupole and octupole excitations of the ^{60}Ni projectile and the ^{89}Y target, their mutual excitations, as well as the two-phonon quadrupole excitation in ^{60}Ni (see Table I). The two approaches differ only in the way fusion is calculated.

The solid curve is based on a real ion-ion potential and ingoing-wave boundary conditions, and the fusion is obtained from the ingoing flux inside the Coulomb barrier, near the local minimum of the interaction potential. This is the conventional method in coupled-channels calculations of fusion reactions [4]. The Woods-Saxon potential used for the nuclear part of the real ion-ion potential has the form

$$U(r,a)=\frac{V_0}{1+\exp\left[\dfrac{r-R}{a}\right]}, \tag{1}$$

with the following values for the parameters: $V_0=77.68$ MeV, $a=0.63$ fm, and $R=9.837$ fm, and a resulting Coulomb barrier of 132.4 MeV. An effective β value is introduced in terms of the reduced matrix element of a deformation amplitude $\alpha_{\lambda\mu}$ (of multipolarity λ and projection μ on the quantization axis) as

$$\beta_\lambda^{eff}=\sqrt{\frac{2\lambda+1}{2I_f+1}}\langle I_f\|\alpha_\lambda\|I_i\rangle=\frac{\sqrt{4\pi(2\lambda+1)B_{W.u.}(E\lambda)}}{(3+\lambda)Z}, \tag{2}$$

where I_i and I_f are the spins of the initial and final states. Here, the result is expressed in terms of the atomic number Z and the reduced transition probability $B(E\lambda)$ (in Weisskopf units). In this way, it is possible to deal on equal footing with transitions in odd and even-even mass nuclei. This effective β value is identical to the usual β value for transitions from the 0^+ ground state of even-even nuclei. From definition (2) we now obtain the matrix element of the deformation amplitude $\alpha_{\lambda\mu}$ between the initial and final states,

$$\begin{aligned}\langle I_fM_f|\alpha_{\lambda\mu}|I_iM_i\rangle&=\langle I_iM_i\lambda\mu|I_fM_f\rangle\frac{\langle I_f\|\alpha_\lambda\|I_i\rangle}{\sqrt{2I_f+1}}\\&=\langle I_iM_i\lambda\mu|I_fM_f\rangle\frac{\beta_\lambda^{eff}}{\sqrt{2\lambda+1}},\end{aligned} \tag{3}$$

where M_i and M_f are the magnetic quantum numbers of the initial and final states, respectively. The two quadrupole transitions in ^{89}Y have been combined into one transition because the two excitation energies are almost identical. The same was done for the two octupole transitions.

The dotted curve in Fig. 1(a) is based on a similar calculation, but it includes an additional short-ranged imaginary potential. The fusion is then obtained as the sum of the absorbed and ingoing flux. These two methods of simulating the fusion process produce almost identical cross sections

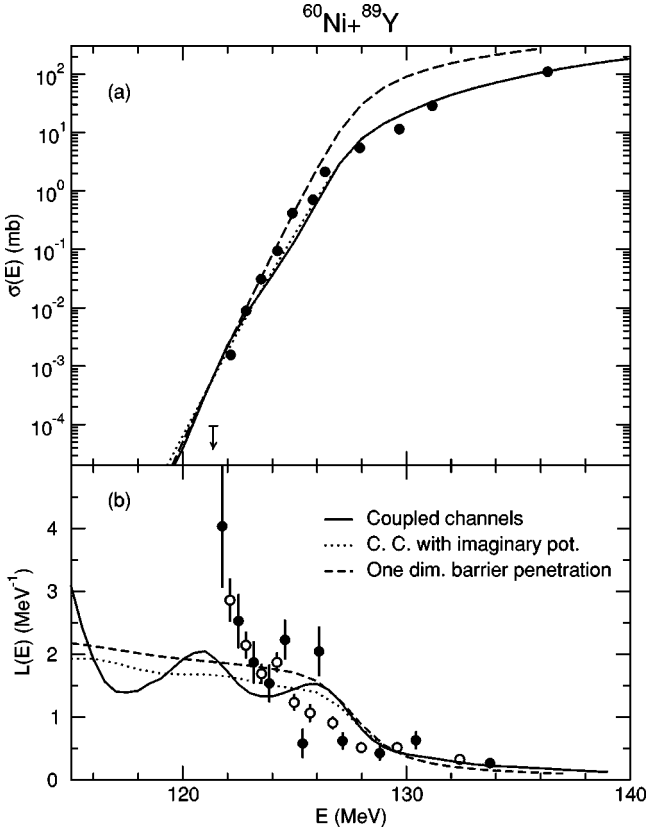

FIG. 1. (a) Fusion excitation function for ^{60}Ni+^{89}Y. The data are from Ref. [1]. The arrow represents an upper limit; (b) logarithmic derivatives for the same system, derived from the data of (a). The solid and dotted curves are the results of the coupled-channels calculations discussed in the text. Also shown are the results for a one-dimensional barrier penetration calculation based on an adjusted interaction (see text for details).

near and above the Coulomb barrier, but there are differences at lower energies, as discussed below. Finally, the dashed curve in Fig. 1(a) is the result of one-dimensional barrier penetration calculations with the same ion-ion potential parameters V_0 and a, but with a radius $R=10.26$ fm adjusted to reproduce the measured data in the 122–126 MeV energy range, resulting in a Coulomb barrier of 127.3 MeV.

The unexpected steep falloff in low-energy fusion cross sections in Ref. [1] was originally analyzed by plotting the logarithmic derivative of the measured fusion cross section σ times the center-of-mass energy E, defined as

$$L(E) = d[\ln(E\sigma)]/dE = \frac{1}{E\sigma}\frac{d(E\sigma)}{dE}. \quad (4)$$

Figure 1(b) compares such derivatives obtained from both the measured fusion cross sections and the three calculations displayed in Fig. 1(a). As discussed in Ref. [1], the experimental results, shown as closed and open circles, were obtained from consecutive data points and from least-squares fits to three data points, respectively. The dashed curve, obtained from the one-dimensional barrier penetration calculation, increases in the vicinity of the Coulomb barrier (set to 127.3 MeV, see above). The rise levels off below the barrier with a more modest increase at lower energies. It should be noted that Wong's formula, used to fit the data in Ref. [1], produces a constant logarithmic derivative at low energies with a value around 1.5 [not shown in Fig. 1(b)].

TABLE I. Low-lying states in ^{60}Ni and ^{89}Y. In the case of ^{60}Ni, the reduced transition rates $B(E\lambda)$ for the quadrupole transitions are from Ref. [25] and the values recommended by Spear [26] are used for the octupole transitions. The $B(E\lambda)$ values for ^{89}Y are from Ref. [27]. The effective β value is defined in Eq. (1).

Nucleus	I_i	I_f	λ	E_f(MeV)	$B_{W.u.}(E\lambda)$	β_λ^{eff}
	0^+	2^+	2	1.333	13.5	0.208
^{60}Ni	2^+	4^+	2	2.506	61.0	0.442
	0^+	3^-	3	4.040	13.9	0.208
	$1/2^-$	$3/2^-$	2	1.507	2.06	0.058
	$1/2^-$	$5/2^-$	2	1.745	2.32	0.062
^{89}Y	$1/2^-$	$5/2^+$	3	2.222	18.3	0.172
	$1/2^-$	$7/2^+$	3	2.530	19.7	0.178
	$1/2^-$	$9/2^+$	5	0.909	5.14	0.085

The solid curve of Fig. 1(b) was obtained from the coupled-channels calculations based solely on a real ion-ion potential. It exhibits an oscillatory behavior below the Coulomb barrier. The oscillations are caused by coupled-channels effects that are damped out when the short-ranged imaginary potential is included (dotted line). The solid curve rises steeply near 115 MeV because of a local minimum in the Coulomb plus nuclear potential inside the barrier at $U_{min}=113.3$ MeV that sets a limit to the fusion process below this threshold. This value may not be realistic since the energy of the ground state of the compound nucleus is much lower, i.e., $-Q=90.5$ MeV. In contrast to the calculations, the data points increase continuously below the Coulomb barrier without any sign of leveling off. The same behavior was observed for four other systems in Ref. [1].

In Ref. [5], it was pointed out that the large logarithmic derivatives obtained from the measurements are consistent with the large diffuseness of the ion-ion potential that these authors have often used to fit high-precision fusion data [6,7]. Their calculations with a large diffuseness of 1.3 fm for the system ^{58}Ni+^{58}Ni do improve the agreement with the data at lower energies when compared to results obtained by using a conventional, more realistic diffuseness of 0.65 fm (see Fig. 3 in Ref. [5]). However, the calculated logarithmic derivative does eventually saturate and exhibit a local maximum. In fact, this maximum may be part of an oscillatory behavior, as seen in Fig. 1(b). The experimental logarithmic derivatives, on the other hand, continue to grow with decreasing energy.

A possible reason for the fact that a large diffuseness is sometimes needed to fit high-precision fusion data could be that the low-energy fusion becomes sensitive to the ion-ion potential inside the Coulomb barrier. This part of the interaction may not be accurately modeled by the conventional Woods-Saxon parametrization in Eq. (1). In order to investigate this point, we have modified the interaction for $r<R$ with a larger diffuseness a_i, but have kept the interaction (1)

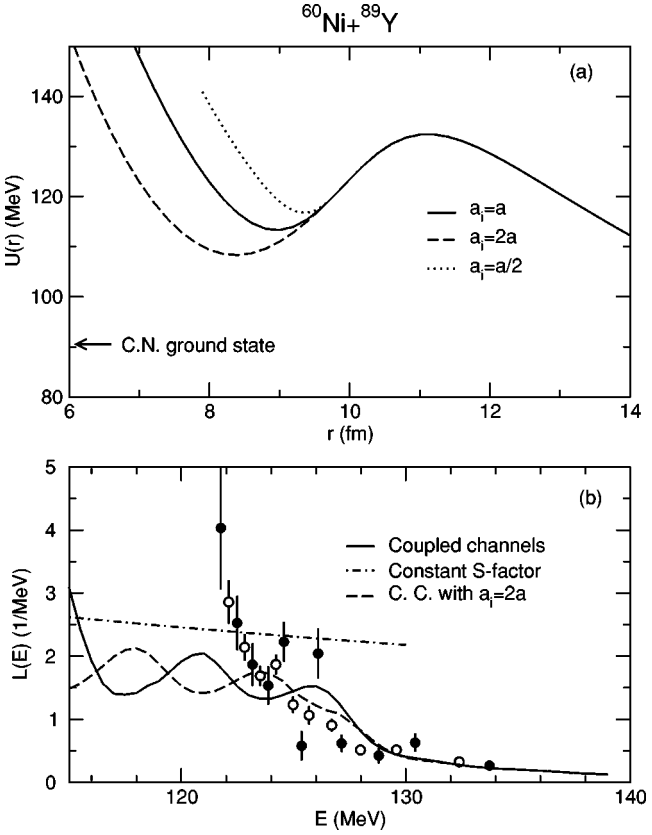

FIG. 2. (a) Ion-ion potentials used in the coupled-channels calculations for ^{60}Ni+^{89}Y. (b) Logarithmic derivatives for the same system. The solid curve is the same as in Fig. 1(b). The dashed curve is the coupled-channels calculations with $a_i=2a$. The dotted-dashed line corresponds to a constant S factor (see text for details).

unchanged for $r>R$, with a diffuseness of $a=0.63$ fm. The specific form for the interior region, in terms of Eq. (1), is

$$U_{int}(r)=\frac{a_i}{a}U(r,a_i)+\frac{1}{2}\left(1-\frac{a_i}{a}\right)V_0 \quad \text{for} \quad r<R. \qquad (5)$$

It should be noted that the two interactions, Eqs. (1) and (5), match up at $r=R$ with a continuous derivative.

Figure 2(b) compares the results of coupled-channels calculations with $a_i=2a$ in Eq. (5) with the conventional Woods-Saxon parametrization [solid curve in both Figs. 1(b) and 2(b)]. It is clear that the new approach improves the agreement with the data in the 122–130 MeV domain. However, at lower energies, the curve develops a maximum and starts oscillating. This trend is similar to that calculated in Ref. [5], but it has been obtained here with a realistic interaction outside the Coulomb barrier. Thus, the new calculations still cannot reproduce the experimental logarithmic derivatives at the lowest energies. For completeness, the total potentials obtained from the Coulomb and the nuclear ion-ion interactions in the two calculations are shown in Fig. 2(a). While the new minimum in the potential energy of $U_{min}=108$ MeV is 5 MeV lower than the previous value, it is still considerably higher than the 90.5 MeV ground state energy of the compound nucleus. In Ref. [8] it has been argued that the failure to reproduce the steep falloff in the ^{60}Ni+^{89}Y system is caused by the Hill-Wheeler approximation for the barrier shape used in the Wong formula. However, as shown in this work and in Ref. [9], coupled-channels calculations, which do not employ this approximation, are also unable to reproduce this feature in the data.

III. *S* FACTOR REPRESENTATION

While the behavior of fusion cross sections at the lowest beam energies is illustrated well by the logarithmic derivatives introduced in Ref. [1] and used in Figs. 1 and 2, we shall show below that an alternative, pragmatic representation is also possible in terms of an S factor. Historically, the S factor was introduced as a useful way of parametrizing cross sections for radiative proton capture, and for light-ion fusion reactions [10,11]. It is defined in terms of the fusion cross section σ as [12]

$$S(E)=E\sigma(E)\exp(2\pi\eta), \qquad (6)$$

where E is the center-of-mass energy, $\eta=Z_1Z_2e^2/(\hbar v)$ is the Sommerfeld parameter, and v is the beam velocity. The Gamow factor $\exp(-2\pi\eta)$ accounts for the main part of the strong energy dependence of the fusion cross section in light-ion reactions, so that the S factor is essentially a constant or exhibits only a weak dependence on energy far below the Coulomb barrier. The ground state Q values for light-ion reactions are usually positive. The reactions can, therefore, in principle take place down to zero center-of-mass energy, and the S factor is often extrapolated to $E=0$.

The S factor for heavy-ion fusion has a very strong energy dependence just below the Coulomb barrier: it increases steeply with decreasing energy (see Fig. 3), reflecting the weaker energy dependence of the $E\sigma(E)$ product when compared to that of the Gamow factor. Nevertheless, the S factor must show a maximum for heavy-ion fusion because it has to reach zero when the reaction Q value is negative. This occurs at the positive center-of-mass energy $E=-Q$, since the ground state of the compound nucleus is reached at this energy. At $E=-Q$, on the other hand, the Gamow factor will still have a finite value. From the definition of the S factor [Eq. (6)], it therefore follows that

$$S(E)\to 0 \quad \text{for} \quad E\to -Q \quad \text{when} \quad -Q>0. \qquad (7)$$

It should be noted that the logarithmic derivatives must eventually go to infinity when $E\to -Q$ as mentioned in Ref. [1]. For light-ion fusion reactions with positive ground state Q values, the lowest entrance channel energy where fusion can take place is evidently $E=0$. At this energy the product $E\sigma$ will go to zero, whereas the inverse Gamow factor $\exp(2\pi\eta)$ will go to infinity. Their product in Eq. (6) may therefore reach a finite value at $E=0$.

The interesting question now is at which energy will the S factor for heavy-ion fusion reach a maximum when the Q value is negative? The examples shown in Fig. 3(a), ^{58}Ni+^{58}Ni [13], ^{60}Ni+^{89}Y [1], ^{90}Zr+^{89}Y, ^{90}Zr+^{90}Zr, and ^{90}Zr+^{92}Zr [14], are the five systems that were discussed in Ref.

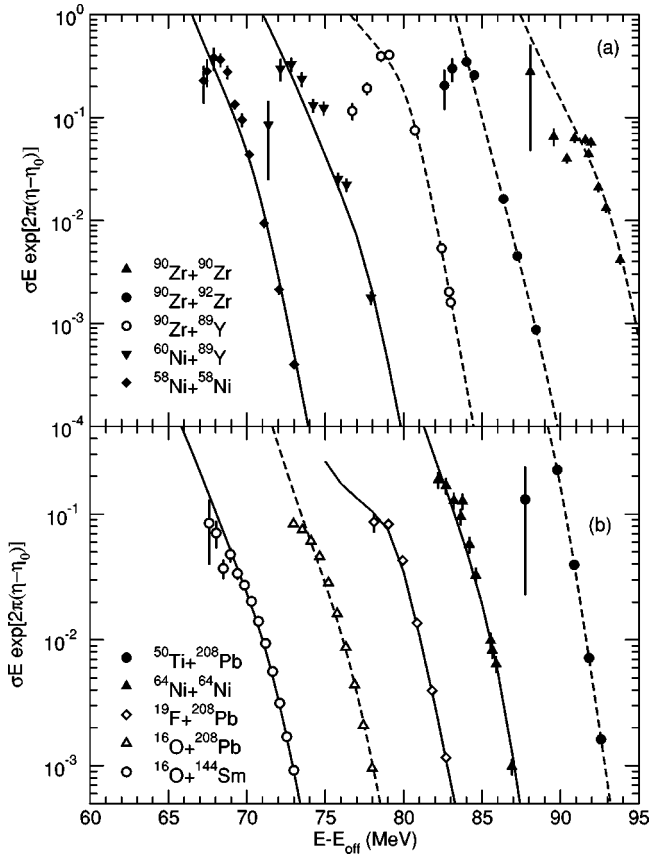

FIG. 3. Plots of the S factors vs $E-E_{off}$. The parameters η_0 and E_{off}(MeV) are used to conveniently place many colliding systems on the same plot. The solid curves are results of coupled-channels calculations, and the dashed curves are fits to the fusion data based on Wong's formula. (a) For systems that have a clear maximum in the S factor at low energy, values of η_0 and E_{off} are 69.26, 26 for ^{58}Ni+^{58}Ni, 92.98, 50 for ^{60}Ni+^{89}Y, 126.02, 92 for ^{90}Zr+^{89}Y, 130.00, 87 for ^{90}Zr+^{92}Zr, 128.24, 84 for ^{90}Zr+^{90}Zr; (b) for systems where the S factor has not quite developed a clear maximum, values of η_0 and E_{off} are 40.10, −11 for ^{16}O+^{144}Sm, 48.41, −3 for ^{16}O +^{208}Pb, 56.30, −3 for ^{19}F+^{208}Pb, 74.20, 7 for ^{64}Ni+^{64}Ni, 126.80, 92 for ^{50}Ti+^{208}Pb, respectively.

[1]. They all exhibit a steep falloff in the fusion cross section at low energies. The solid curves are the results of coupled-channels calculations discussed in Ref. [1] and above (for the system ^{60}Ni+^{89}Y calculations with $a_i=2a$ are shown). The dashed curves are fits to the data at higher energies based on Wong's formula which was used in Ref. [1] for those systems where coupled-channels calculations are not available. It is seen in Fig. 3(a) that the data for these systems all develop a maximum in the S factor at low energies. For the system ^{90}Zr+^{90}Zr, there appears to be a steep increase at the lowest energies, below the local maximum. This behavior might be caused by a small target contamination from heavier Zr isotopes as discussed in Ref. [1]. According to Eq. (7), the maximum of the S factor has to occur at a definite energy, but it is again surprising that it corresponds to a rather large excitation energy in the compound nucleus, in the range of 20–30 MeV, where the associated level density remains very large. There is evidently some mechanism that hinders the fusion process at these high excitation energies. In Ref. [1], it was suggested that, because of the high excitation energy, the hindrance might be an entrance channel phenomenon rather than a compound nucleus effect. However, to the best of our knowledge, a model calculation resulting in a maximum of the S factor at these high excitation energies in the compound nucleus has not yet been proposed.

IV. SYSTEMATICS OF LOW-ENERGY DATA

The relation between the two representations of the low-energy fusion data, namely, the S factor and the logarithmic derivative, can be understood by looking at the derivative of the S factor. From Eqs. (4) and (6), one obtains the following expression:

$$\frac{dS}{dE} = S(E)\left[L(E) - \frac{\pi\eta}{E}\right]. \tag{8}$$

A maximum in the S factor implies that $dS/dE=0$. This is fulfilled when the logarithmic derivative is

$$L_{CS}(E) = \frac{\pi\eta}{E} = \frac{\pi Z_1 Z_2 e^2}{E^{3/2}}\sqrt{\frac{m_N}{2}\frac{A_1 A_2}{A_1+A_2}}, \tag{9}$$

where A_1 and A_2 are the mass numbers of the reaction partners and m_N is the nucleon mass. This function, which is the logarithmic derivative for a constant S factor, is shown by the dotted-dashed curve in Fig. 2(b). The logarithmic derivative $L(E)$ extracted from the experimental data will intersect the curve $L_{CS}(E)$ exactly at the energy where the experimental S factor exhibits a maximum in Fig. 3(a). Let us denote the energy and logarithmic derivative where this intersection occurs by E_s and $L_s=L(E_s)$, respectively. These two quantities are then related by the equation

$$L_s = \frac{\pi Z_1 Z_2 e^2}{E_s^{3/2}}\sqrt{\frac{m_N}{2}\frac{A_1 A_2}{A_1+A_2}}, \tag{10}$$

since they fall on the curve defined in Eq. (9).

There is nothing particularly special about the S factor, nor about the values E_s and L_s where the logarithmic derivative extracted from measurements intersects with the logarithmic derivative for a constant S factor. It is simply an alternative, convenient way of characterizing the unexpected steep falloff of the measured fusion cross sections. Thus, when the S factor reaches a maximum, the logarithmic derivative will have reached a value that exceeds the expectations based on the coupled-channels calculations. The values E_0 obtained in Ref. [1] are close to the corresponding values of E_s. The advantage of the S factor is that it gives a simple and direct representation of the fusion cross section, whereas the logarithmic derivatives [Eq. (4)] and also the so-called barrier distributions [15] are more indirectly derived quantities. Moreover, the energy E_0, which was defined in Ref. [1], is model dependent, while E_s and L_s are obtained without free parameters.

It turns out that the value of L_s is nearly identical for all five systems shown in Fig. 3(a), with an average value of 2.33 MeV^{-1} (see Table II, category I). Assuming that

TABLE II. The parameter $\zeta = Z_1 Z_2 \sqrt{A_1 A_2/(A_1+A_2)}$, the energy E_s, and the logarithmic derivative L_s, which characterize the maximum of the S factor for different systems. Also given are the lowest measured energy (E_{min}) and the corresponding cross section (σ_{min}). The first category of systems exhibits a clear maximum in the S factor. In the second category, a maximum has not quite been reached, but can be estimated by extrapolating the logarithmic slope to the value for a constant S factor. In the third category, there is no clear sign of a maximum in the S factor.

System	ζ	E_s(MeV)	L_s(/MeV)	E_{min}(MeV)	$\sigma_{min}(\Delta\sigma)(\mu$b)	Ref.
Category I						
^{58}Ni+^{58}Ni	4222	94.0	2.29	93.3	49 (20)	[13]
^{60}Ni+^{89}Y	6537	122.9	2.37	121.4	$<$0.09	[1]
^{90}Zr+^{89}Y	10436	170.8	2.31	168.7	0.34 (0.07)	[14]
^{90}Zr+^{90}Zr	10733	175.2	2.29	172.1	0.08 (0.07)	[14]
^{90}Zr+^{92}Zr	10792	170.7	2.40	169.6	0.12 (0.05)	[14]
Category II						
^{16}O+^{144}Sm	1882	57.7	2.13	56.6	150 (80)	[6]
^{16}O+^{208}Pb	2529	69.6	2.15	70.0	240 (10)	[19]
^{19}F+^{208}Pb	3079	75.5	2.32	75.1	23 (4)	[17]
^{40}Ca+^{90}Zr	4210	93.2	2.32	93.4	840 (160)	[20]
^{64}Ni+^{64}Ni	4435	89.0	2.61	89.2	16.8 (4.0)	[18]
^{50}Ti+^{208}Pb	11454	181.2	2.32	179.8	0.00001	[16]
Category III						
^{19}F+^{232}Th	3394			70.5	0.58 (0.08)	[21]
^{40}Ca+^{96}Zr	4251			91.7	41 (6)	[20]
^{40}Ar+^{116}Sn	4908			95.7	3.8 (1.1)	[23]
^{64}Ni+^{74}Ge	5249			97.5	13.3 (3.3)	[22]
^{40}Ar+^{148}Sm	6262			112.7	0.8 (0.5)	[23]
^{40}Ar+^{154}Sm	6289			108.8	1.6 (0.9)	[23]
^{86}Kr+^{76}Ge	7317			120.7	6.8 (5.5)	[24]
^{86}Kr+^{100}Mo	10281			155.4	14.4 (1.5)	[24]
^{86}Kr+^{104}Ru	10868			162.4	4.9 (0.8)	[24]

2.33 MeV^{-1} is a "universal" value, Eq. (10) can be used to derive an analytic expression for the energy E_s. Thus, inserting the value $L_s = 2.33$ MeV^{-1} into Eq. (10), we obtain

$$E_s = 0.356\left[Z_1 Z_2 \sqrt{\frac{A_1 A_2}{A_1 + A_2}}\right]^{2/3} (\text{MeV}). \qquad (11)$$

This expression is given by the solid curve in Fig. 4. The solid points are the values E_s obtained for the five systems mentioned above. A common feature of these five systems is that the reacting nuclei are all rather stiff.

There are other measurements in the literature where the S factor has not quite reached a well-defined maximum, but starts to deviate at the lowest energies from the calculations based on coupled-channels or on Wong's formula. There is even some evidence for a maximum in one or two cases. Examples are ^{50}Ti+^{208}Pb [16], ^{19}F+^{208}Pb [17], ^{64}Ni+^{64}Ni [18], ^{16}O+^{208}Pb [19], ^{16}O+^{144}Sm [6] and ^{40}Ca+^{90}Zr [20]. These systems are also included in Table II under category II, and some are displayed in Fig. 3(b) as well. The solid curves represent the coupled-channels calculations reported in the original references. The behavior for ^{16}O+^{144}Sm and ^{40}Ca+^{90}Zr at the lowest energies is similar to that seen for ^{90}Zr+^{90}Zr which, as mentioned before, might be due to small contaminations by heavier isotopes in the target. The triangles in Fig. 4 are estimated values of E_s obtained by extrapolating the logarithmic derivatives of the measurements to the point where they intersect the curve L_{CS} for a constant S factor, defined in Eq. (9). The estimated values of E_s are in reasonable agreement with the solid curve, except perhaps for the system ^{64}Ni+^{64}Ni [18], where the estimated value is below the curve. It is worth noting that this system is softer than the one studied via the ^{58}Ni+^{58}Ni reaction.

Experiments with "softer" or well-deformed nuclei have usually not been performed at sufficiently low energies to extend into the region where the S factor exhibits a maximum. This may not be so surprising since the strong coupled-channels effects, typical for softer or well-deformed nuclei, tend to broaden the effective barrier distribution [15] and push the energy where the steep rise in the logarithmic derivative occurs down to even lower energies. Examples of systems where stronger couplings play a role are ^{19}F+^{232}Th [21], ^{40}Ca+^{96}Zr [20], ^{64}Ni+^{74}Ge [22], ^{40}Ar+^{116}Sn, ^{40}Ar+^{148}Sm, ^{40}Ar+^{154}Sm [23], and ^{86}Kr+^{76}Ge, ^{86}Kr+^{100}Mo, ^{86}Kr+^{104}Ru [24]. These systems are also included in Table II under category III. The open circles in Fig. 4 are

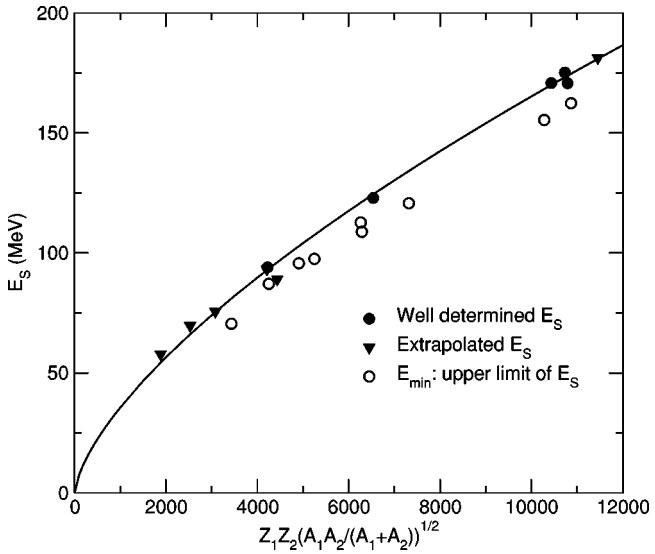

FIG. 4. Systematics of the energy E_s where the S factor has a maximum as a function of the parameter, $Z_1Z_2\sqrt{A_1A_2/(A_1+A_2)}$. The solid curve is calculated with the empirical expression given by Eq. (11). The solid points were obtained for systems that exhibit a clear maximum in the S factor (category I in Table II). The triangles were obtained by extrapolating the logarithmic derivative to the value for a constant S factor, Eq. (9). The open circles show the lowest measured energy E_{min} for those systems where no sign of a maximum in the S factor has been found so far.

upper limits for the corresponding E_s values and represent the lowest energy where measurements have been performed.

The experimental data referenced in the discussions above and in Ref. [1] are mostly cross sections for fusion evaporation. For the $^{19}F+^{208}Pb$ [17] and $^{16}O+^{208}Pb$ reactions [19], total fusion cross sections are available. Fission is the main contributor to fusion for these two systems even at lowest energies. It thus appears that the behavior discussed above is present for both fusion-evaporation and fusion-fission reactions.

V. CONCLUSIONS

To summarize, our investigations show that the S factor is a convenient representation of fusion cross sections for heavy-ion systems at extreme sub-barrier energies. The S factor reveals through the presence of a maximum in the S vs E curve the unexpected steep falloff in cross section reported previously. By combining the two representations, the logarithmic derivative and the S factor, we were able to derive a simple empirical formula for the energy where the S factor develops its maximum for reactions with stiff partners.

The coupled-channels calculations presented here demonstrate that the low-energy behavior of heavy-ion fusion cross sections is sensitive to the way fusion is defined, with or without an imaginary potential. Moreover, the low-energy behavior is also sensitive to the parametrization of the ion-ion potential inside the Coulomb barrier, and the conventional Woods-Saxon form may not be best suited for a realistic description. At present, coupled-channels calculations have not been able to reproduce the data down to the lowest energies. On the experimental side, it is clearly of interest to measure fusion cross sections down to even lower energies, especially for softer colliding systems, in order to investigate whether the experimental logarithmic derivative keeps increasing, exhibits a maximum, or starts oscillating.

ACKNOWLEDGMENT

This work was supported by the U.S. Department of Energy, Nuclear Physics Division, under Contract No. W-31-109-ENG.

[1] C. L. Jiang *et al.*, Phys. Rev. Lett. **89**, 052701 (2002).
[2] H. Esbensen and S. Landowne, Phys. Rev. C **35**, 2090 (1987).
[3] C. Y. Wong, Phys. Rev. Lett. **31**, 766 (1973).
[4] A. B. Balantekin and N. Takigawa, Rev. Mod. Phys. **70**, 77 (1998).
[5] K. Hagino, N. Rowley, and M. Dasgupta, Phys. Rev. C **67**, 054603 (2003).
[6] J. R. Leigh *et al.*, Phys. Rev. C **52**, 3151 (1995); H. Esbensen *et al.*, *ibid.* **54**, 3109 (1996).
[7] J. O. Newton, C. R. Morton, M. Dasgupta, J. R. Leigh, J. C. Mein, D. J. Hinde, H. Timmers, and K. Hagino, Phys. Rev. C **64**, 064608 (2001).
[8] C. J. Lin, Phys. Rev. Lett. **91**, 229201 (2003).
[9] C. L. Jiang *et al.*, Phys. Rev. Lett. **91**, 229202 (2003).
[10] S. E. Woosley *et al.*, At. Data Nucl. Data Tables **22**, 371 (1978).
[11] S. Schramm *et al.*, Astrophys. J. **127**, 296 (1990).
[12] E. M. Burbridge *et al.*, Rev. Mod. Phys. **29**, 547 (1957).
[13] M. Beckerman *et al.*, Phys. Rev. C **23**, 1581 (1982).
[14] J. G. Keller *et al.*, Nucl. Phys. **A452**, 173 (1986).
[15] N. Rowley, G. R. Satchler, and P. H. Stelson, Phys. Lett. B **254**, 25 (1991).
[16] S. Hofman *et al.*, Z. Phys. A **358**, 377 (1997).
[17] D. J. Hinde *et al.*, Phys. Rev. C **60**, 054602 (1999); see also D. J. Hinde *et al.*, in *Tours Symposium on Nuclear Physics III*, edited by M. Arnould, M. Lewitowicz, Yu. Ts. Oganessian, M. Ohta, H. Utsunomiya, and T. Woda, AIP Conf. Proc. No. 425 (AIP, Woodbury, NY, 1998), p. 223.
[18] D. Ackermann *et al.*, Nucl. Phys. **A609**, 91 (1996).
[19] C. R. Morton *et al.*, Phys. Rev. C **60**, 044608 (1999).
[20] H. Timmers *et al.*, Nucl. Phys. **A633**, 421 (1998).
[21] D. M. Nadkarni *et al.*, Phys. Rev. C **59**, R580 (1999).
[22] M. Beckerman *et al.*, Phys. Rev. C **25**, 837 (1982).
[23] W. Reisdorf *et al.*, Nucl. Phys. **A438**, 212 (1985).
[24] W. Reisdorf *et al.*, Nucl. Phys. **A444**, 154 (1985).
[25] M. M. King, Nucl. Data Sheets **69**, 1 (1993).
[26] R. H. Spear, At. Data Nucl. Data Tables **42**, 55 (1989).
[27] B. Singh, Nucl. Data Sheets **85**, 1 (1998).